Agricultural Water Management 329 (2026) 110381

Contents lists available at ScienceDirect

Agricultural Water Management

journal homepage: www.elsevier.com/locate/agwat

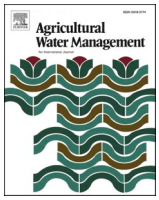

When floods heal or harm after drought: Three archetypes of maize photosynthetic response to drought-to-flood transitions across China

Peng Li [a,b], Sen Chen [b], Liang He [c,*], Ning Yao [d], Chao Wang [a], Meichen Feng [a], Xingyu Hao [a,*], Jianqiang He [d], Qiang Yu [a,*]

[a] College of Agriculture, Shanxi Agricultural University, Taigu, Shanxi 030801, China
[b] College of Natural Resources and Environment, Northwest A&F University, Yangling, Shaanxi 712100, China
[c] National Meteorological Centre, Beijing 100081, China
[d] College of Water Resources and Architectural Engineering, Key Lab of Agricultural Soil and Water Engineering in Arid and Semiarid Areas, Ministry of Education, Northwest Agriculture and Forestry University, Yangling, Shaanxi 712100, China

ARTICLE INFO

Keywords:
Compound hydroclimatic extremes
Gross primary productivity
Compound resistance
Soil moisture
SHAP analysis

ABSTRACT

Drought-to-flood transitions (DTF) show regional contrasts across China's major maize-producing regions, yet whether the flood phase mitigates or compounds drought impacts remains unresolved. 1-km observations (2000–2019) are used to identify soil-moisture-defined DTF and track canopy function with 8-day gross primary productivity (GPP) percentiles. Responses are quantified with two metrics: Compound Resistance (CR; whole-sequence GPP suppression) and Resistance Difference (RD; flood-phase effect beyond drought legacy; RD>0 mitigation, RD<0 compounding). Three vulnerability archetypes clarify flood-phase effects on drought legacy. Across climatic gradients, outcomes depend on the hydrothermal window: low-energy (cool/cloudy) and/or waterlogging-prone rewetting tends to compound drought legacy, whereas warm, energy-favorable rewetting promotes recovery. A compounding stress trap characterizes the Northern Arid–Semiarid Region, where exposure is highest (1.2 events per unit area) and impactful events (drought-stage GPP suppression) are numerous (5150). Random Forest–SHAP shows flood-phase solar radiation and temperature limit recovery and CR, while RD varies with drought-stage constraints and climate background. The Northeast China Plain shows a conditional response: events are frequent (5033) and impactful events increase over 2000–2019 ($p < 0.01$), while RD spans both signs, indicating that flooding can offset or deepen drought impacts depending on flood-phase solar radiation and temperature. The Yunnan–Guizhou Plateau exhibits buffered recovery: events remain long (mean duration 63 days), events are fewer (3019) yet impactful events increase over 2000–2019 ($p < 0.001$), and RD is predominantly positive, consistent with longer flood duration and favorable flood-phase energy conditions supporting rebound. These archetypes clarify when flooding mitigates or compounds drought legacy, informing region-specific adaptation.

1. Introduction

Post-drought floods are not universally beneficial: they can either accelerate recovery or lock crops into prolonged suppression. Anthropogenic climate change, driven by rising atmospheric CO_2 concentrations, is intensifying the global hydrological cycle and reshaping terrestrial carbon–water dynamics, thereby amplifying hydroclimatic variability (Gu et al., 2025; Li et al., 2022; Piao et al., 2019; Sun et al., 2025). One emerging manifestation is the increasing frequency of abrupt drought-to-flood transitions (DTF), defined as rapid within-season shifts from drought to flood conditions (Shi et al., 2021; Wang et al., 2025; Zheng et al., 2025). Recent studies have demonstrated that such transitions are not uniform across regions; their impacts vary significantly due to factors such as urbanization, water management, and local climatic conditions, which can intensify the effects of DTF events (Huang et al., 2026; Ning et al., 2026). Such transitions disrupt vegetation function and biomass allocation (Bi et al., 2023b) and can be particularly damaging to croplands, which show higher sensitivity than forests and shrublands (Zhang et al., 2025). Therefore, a central question for climate-risk management and food security is not only where DTF

* Corresponding authors.
E-mail addresses: heliang@cma.gov.cn (L. He), haoxingyu1976@126.com (X. Hao), yuq@igsnrr.ac.cn (Q. Yu).

https://doi.org/10.1016/j.agwat.2026.110381
Received 14 January 2026; Received in revised form 21 March 2026; Accepted 21 April 2026
Available online 23 April 2026

occurs, but when and how the flood phase alleviates drought legacy versus compounds stress.

Research on DTF has evolved from descriptive case studies toward operational event detection. Existing definitions typically reflect the primary indicator and its intended application, encompassing meteorological (precipitation-based), hydrological (streamflow-based), and agricultural types. For assessing agricultural impacts, the most relevant approach diagnoses DTF from land-surface water balance variables, where root-zone soil moisture is widely used as a direct proxy for plant water status (Bai et al., 2023; Qiu et al., 2024). Across approaches, two attributes are consistently emphasized: alternation between drought and flood states and the abruptness of the transition, which is commonly implemented using thresholds and/or change-point detection (Bai et al., 2024; Tu et al., 2022). However, recent studies have shown that the definition of DTF events is highly dependent on the thresholds and time scales used, which can significantly alter event detection and timing, thus affecting impact assessment (Anderson et al., 2025). Recent multivariate frameworks further integrate precipitation and evapotranspiration with soil moisture to improve event representation (Bai et al., 2024). At regional scales, studies report pronounced spatial heterogeneity in DTF events across China, with recurrent hotspots in core agricultural regions such as the North China Plain and Yangtze River basins; a synthesis of this research further reveals a clear intensification trend in recent decades—evident in increasing frequency and spatial coverage—that is primarily driven by anthropogenic forcing and modulated by large-scale climate variability (Bi et al., 2023a; Chan et al., 2018; Li et al., 2022; Liang et al., 2025; Zhang et al., 2023). For instance, urbanization has been shown to significantly amplify the frequency and severity of drought-to-flood transitions, especially in rapidly expanding urban fringe areas (Huang et al., 2026). Collectively, these advances improve our ability to map DTF hazards, but they do not explain where DTF translates into sustained photosynthetic suppression—or why impacts diverge across agro-ecological contexts (Peduzzi et al., 2009; Ward et al., 2020).

Evidence from plot-scale experiments confirms that DTF events suppress crop biomass and yield, trigger physiological disruptions such as reduced photosynthesis and accelerated senescence, and may exacerbate environmental externalities including elevated nitrogen and phosphorus losses (Bi et al., 2025; Gao et al., 2019; Xiong et al., 2018; Yuan et al., 2024). Critically, the combined effect of sequential drought and flood is not merely additive; outcomes range from antagonistic (where mild drought partially offsets subsequent flood damage) to synergistic, depending on stress intensity and timing (Gao et al., 2017; Xu et al., 2021). However, the degree to which these effects are modulated by human water management practices, such as irrigation and water reservoir regulation, remains underexplored (Götte and Brunner, 2024). Besides, translating these process-level insights into predictive understanding at regional scales remains challenging. Similar DTF regimes can yield markedly different photosynthetic responses across agro-ecological contexts, because crop responses are conditioned by antecedent stress, phenological stage, and the interplay of energy, water, and temperature constraints during each event phase (Jacques et al., 2021; Pissolato et al., 2024; Toca et al., 2025). Recent work has highlighted that such responses are not only biophysically driven but also influenced by socio-economic factors such as irrigation availability, infrastructure, and management practices, which modulate crop vulnerability in specific regions (Matanó et al., 2022). Thus, the key challenge is to diagnose, at scale, how phase-specific conditions shape canopy suppression trajectories through the drought–flood sequence, rather than treating DTF exposure as a sufficient proxy for impact.

A central uncertainty underpinning this scaling challenge is the net effect of the flood phase: whether post-drought rewetting primarily alleviates water deficit and aids recovery, or exacerbates stress through mechanisms such as waterlogging and associated constraints (Huang et al., 2019). This net effect is expected to vary geographically, with studies showing that the flood-phase contribution to crop recovery is often contingent on large-scale climatic patterns and regional water management practices (Zhang et al., 2026). The sign and magnitude of this flood-phase contribution are expected to vary geographically (Zhang et al., 2023), yet existing methodologies—relying largely on site experiments or end-of-season yield metrics—struggle to isolate the drought legacy from flood-stage modulation (Hao et al., 2022). For maize, we still lack a scalable way to track photosynthetic function through the full drought–flood sequence while separating whole-event suppression from the flood phase's net contribution, limiting our ability to predict where and why vulnerability concentrates.

To bridge these knowledge gaps, we establish a three-part analytical framework to assess maize vulnerability to DTF across major agricultural zones in China. First, at the 1-km pixel scale during maize growing seasons (2000–2019), we identify root-zone soil-moisture-defined DTF events that satisfy both state alternation and abruptness, aligning hazard detection with crop-relevant water availability. Second, we quantify event-scale canopy carbon-uptake responses using remotely sensed GPP as a proxy for canopy photosynthetic activity, and distill them into two complementary metrics derived from percentile-transformed GPP: compound resistance (CR), capturing integrated suppression over the full drought–flood sequence, and resistance difference (RD), isolating the net contribution of the flood stage to diagnose whether flooding amplifies or alleviates drought legacy. Conceptually, CR summarizes whole-event suppression, whereas RD isolates the flood-phase net effect (mitigation versus compounding). Third, we employ SHAP-interpreted random forest models to attribute the spatial heterogeneity of CR and RD to event traits, phase-specific meteorology, large-scale climate, phenology, and environmental context. Building on this process-resolved attribution, we further synthesize DTF exposure, CR, and RD into a typology of vulnerability pathways—compounding-trap, conditional-response, and buffered-recovery—to connect "where DTF occurs" with "how crops respond" and "which constraints dominate". By linking event detection, impact quantification, phase-resolved attribution, and archetype synthesis, this study provides a scalable basis for diagnosing regional risk and prioritizing region-tailored adaptation across China's maize belt.

2. Materials and methods

2.1. Study area and agricultural zoning

This study focuses on China’s major maize-producing regions, which span pronounced climatic and agro-ecological gradients. To facilitate regional comparison of DTF impacts and their drivers, we adopted a nine-zone agricultural classification system from the Resource and Environment Science and Data Center (RESDC) (Fig. 1), including the Northeast China Plain (Zone A), the Northern Arid–Semiarid Region (Zone B), the North China Plain (Zone C), the Loess Plateau (Zone D), the Qinghai–Tibet Plateau (Zone E), the Middle–Lower Yangtze Plain (Zone F), the Sichuan Basin (Zone G), Southern China (Zone H), and the Yunnan–Guizhou Plateau (Zone I). This zoning captures major differences in cropping systems, irrigation intensity, and climatic exposure (Han et al., 2024).

All analyses were restricted to cropland pixels identified as stable maize-growing areas, defined as pixels with maize records in at least 10 years. After this screening, only 7 valid pixels remained in Zone E and 3 in Zone H; these sample sizes were considered insufficient for robust zonal analysis, and both zones were therefore excluded. The final analysis thus focused on seven major maize-producing zones. In addition, the maize distribution dataset used here covers mainland China only; Taiwan was not included because corresponding source data were unavailable.

2.2. Data sources and preprocessing

Our analytical framework integrates five groups of data to establish a

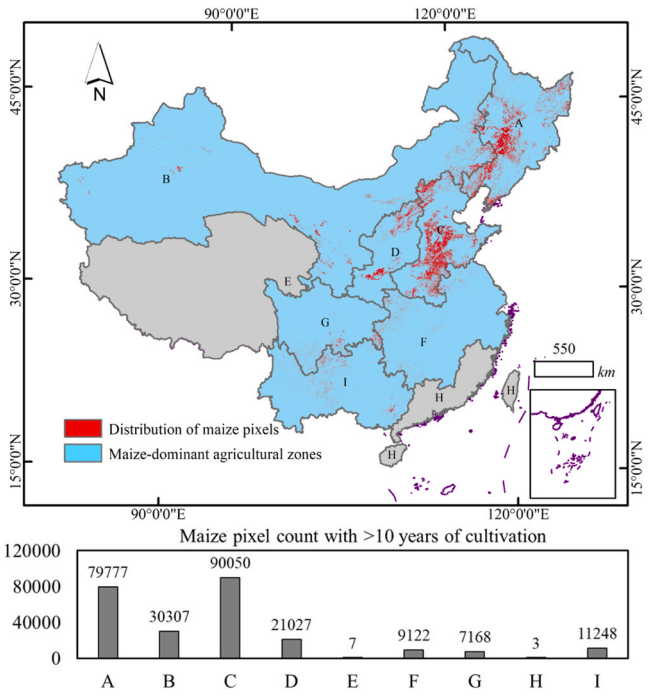

Fig. 1. Geographic distribution of China's major maize-producing regions and maize pixels with > 10 years of cultivation.

complete diagnostic chain from hazard detection to impact attribution: maize distribution and phenology, root-zone soil moisture, gross primary productivity (GPP), meteorological variables and climate indices, and static environmental/management factors. The corresponding dataset sources are listed in Table 1.

2.2.1. Maize distribution and phenology

We used the ChinaCropPhen1km dataset (Luo et al., 2020) to delineate maize-growing areas and pixel-specific growing seasons. Only grid cells with stable maize cultivation (≥10 years of planting records) were retained. Key phenological stages (three-leaf, heading, and maturity) were used to temporally align our analyses and to categorize events as pre- or post-heading.

2.2.2. Root-zone soil moisture

To represent crop-relevant water availability, we used root-zone soil moisture from the SMCI1.0 dataset (Soil Moisture of China by in situ data, version 1.0; Li et al., 2022). A depth-weighted mean soil moisture was calculated for the 0–60 cm layer, corresponding to the main rooting zone of maize. Daily soil moisture data were then aggregated to 8-day intervals for subsequent event identification.

Table 1
Main datasets used in this study.

Data category	Dataset / source
Maize distribution and phenology	ChinaCropPhen1km (Luo et al., 2020) https://doi.org/10.6084/m9.figshare.8313530
Root-zone soil moisture	SMCI1.0 (Li et al., 2022) https://doi.org/10.11888/Terre.tpdc.272415
Gross primary productivity	PML_V2.2a (Zhang et al., 2019) https://developers.google.com/earth-engine/datasets
Meteorological variables	CMFD v2.0 https://cstr.cn/18406.11.Atmos.tpdc.302088
Climate index	The Southern Oscillation Index (SOI) https://www.cpc.ncep.noaa.gov/data/indices/soi
Soil properties	CSDLv2 (Shi et al., 2025) https://doi.org/10.11888/Terre.tpdc.301235
Topography	Digital elevation model of China https://data.tpdc.ac.cn/zh-hans/data/12e91073–0181–44bf-8308-c50e5bd9a734
Irrigation status	CIrrMap250 (Zhang et al., 2024) https://doi.org/10.6084/m9.figshare.24814293.v2

2.2.3. Gross primary productivity (GPP) and percentile transformation

We used 8-day GPP data from the PML_V2.2a product (Zhang et al., 2019), harmonized to the common 1-km analysis grid. Because absolute GPP levels differ substantially across China's maize-growing regions, we processed the GPP time series at each pixel to emphasize event-scale anomalies rather than raw productivity values. Specifically, a long-term linear trend was first removed from the 8-day GPP series, after which the mean seasonal cycle for each calendar 8-day period during 2000–2019 was also subtracted. The resulting residuals were then converted to percentile ranks (0–100) for each calendar 8-day period relative to the corresponding interannual distribution at the same pixel, following Forzieri et al. (2022). This detrending and percentile transformation reduced the influence of long-term change and recurring seasonal variability while retaining anomalous fluctuations associated with DTF events. The processed GPP percentile series was subsequently used to quantify event-scale canopy photosynthetic responses.

2.2.4. Meteorological variables and climate indices

High-resolution gridded precipitation, solar radiation, and air temperature were obtained from CMFD v2.0 (He et al., 2020) and aggregated to 8-day intervals. For each identified DTF event, these meteorological variables were summarized separately for the drought and flood phases in order to represent phase-specific environmental constraints. The Southern Oscillation Index (SOI) was obtained from the NOAA Climate Prediction Center (CPC) as a monthly large-scale climate indicator. The SOI is a standardized index based on the observed sea level pressure difference between Tahiti and Darwin, Australia. Event-period and pre-event mean SOI values were then derived to represent the broader climate background associated with each DTF event.

2.2.5. Static environmental and management factors

We incorporated data on soil properties (silt, clay, and porosity from CSDLv2; Shi et al., 2025), topography (elevation and slope derived from the Digital Elevation Model of China provided by the National Tibetan Plateau Data Center, Third Pole Environment Data Center), and irrigation status (rainfed vs. irrigated from CIrrMap250; Zhang et al., 2024). All static datasets were harmonized to a common 1-km grid. Higher-resolution datasets were aggregated to 1 km using mean values within each target pixel.

2.3. Identification of abrupt DTF events

We defined a drought-to-flood transition (DTF) event as a rapid within-season shift from a sustained drought state to a subsequent flood state at a 1-km maize pixel. Because robust state identification and rapid-transition detection require different temporal support, we adopted a dual-timescale framework: 8-day root-zone soil moisture was used to identify drought and flood states, whereas daily soil moisture was used to confirm abrupt transition timing.

Event identification followed three sequential steps (Fig. 2). First, the 8-day root-zone soil moisture series was standardized into a Standardized Soil Moisture Index (SSMI, Konkathi and Karthikeyan, 2024; Li et al., 2025) to express dry and wet anomalies relative to local historical conditions. Drought was defined as SSMI ≤ -0.5 and flood as SSMI $\geq +0.5$. To ensure persistent hydrological states while preserving agriculturally relevant rapid transitions, only drought episodes lasting at least 16 days and flood episodes lasting at least 8 days were retained. A candidate DTF event was defined when a flood episode immediately followed a drought episode.

Second, abruptness was confirmed using the Soil Moisture Concentration Index (SMCI) calculated from daily soil moisture within a

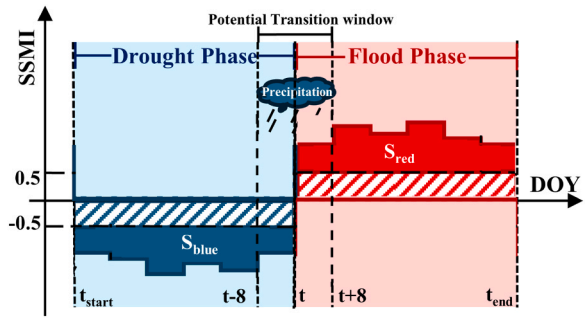

Fig. 2. Conceptual schematic of the soil moisture–based identification of DTF events.

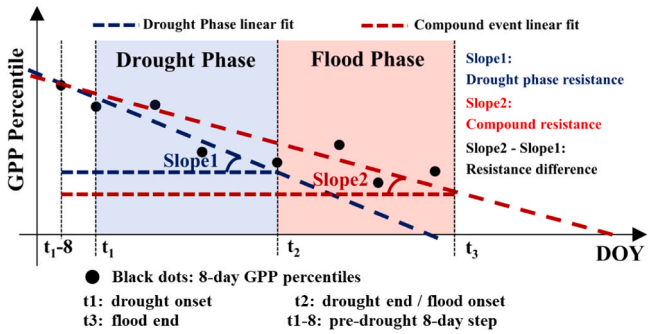

Fig. 3. Schematic framework for quantifying drought-phase resistance, CR, and RD from GPP percentiles.

centered sliding window (T = 7 days), following Qiu et al. (2024). Candidate transition dates were identified as local minima in the SMCI series that exceeded a pixel-specific wetting threshold derived from the local SMCI distribution. Using daily soil moisture at this step allowed rapid wetting signals to be detected even though drought and flood states were screened from 8-day composites.

Third, a precipitation consistency check was applied to exclude pseudo-transitions unsupported by a meteorological wetting signal. Specifically, mean precipitation during the transition window was required to exceed that during an equal-length pre-drought reference window. Only events satisfying all three criteria were retained as abrupt DTF events.

For each retained event, frequency, intensity, and duration were summarized by agricultural zone, and temporal trends were assessed using Sen's slope estimator and the Mann–Kendall test (Hamed and Ramachandra Rao, 1998). Additional technical details on SSMI construction, SMCI calculation, and the full event-identification workflow are provided in Supplementary Texts S1, S2, and S3.

2.4. Quantifying crop response: definitions of compound resistance (CR) and resistance difference (RD)

To diagnose maize photosynthetic vulnerability to DTF, we quantified event-scale canopy response using two complementary metrics derived from the processed GPP percentile series.

We first defined crop-impactful events as those in which the drought phase produced a clear initial photosynthetic decline, indicated by a negative slope from the pre-drought baseline to the drought end. To avoid using events that started from already depressed productivity conditions, events with a pre-drought GPP percentile $\leq 40\%$ were excluded, following Zhang et al. (2025). The remaining events were considered suitable for evaluating canopy response to sequential drought–flood stress.

For each crop-impactful event, resistance was quantified as the slope of GPP percentile decline over a specified interval. Drought-phase resistance ($Slope_1$) was defined as the decline rate from the pre-drought baseline to the end of the drought phase. Compound Resistance (CR) was defined as the decline rate over the entire drought–flood sequence. A more negative CR indicates stronger overall photosynthetic suppression. Resistance Difference (RD) was calculated as $RD = CR - Slope_1$, thereby isolating the net contribution of the flood phase. A positive RD indicates that flooding partially alleviated the drought legacy, whereas a negative RD indicates that flooding further aggravated suppression.

Conceptually, CR summarizes whole-event suppression, whereas RD isolates the role of the flood phase in modulating drought legacy (Fig. 3). Temporal trends in crop-impactful event frequency, CR, and RD were analyzed using Sen's slope estimator and the Mann-Kendall test.

2.5. Attribution analysis: random forest and SHAP interpretation

To explain the spatial heterogeneity in CR and RD, we employed Random Forest regression models interpreted using SHapley Additive exPlanations (SHAP) (Ge et al., 2025; Xie et al., 2025). This framework is well suited for capturing nonlinear relationships and threshold-like responses between crop vulnerability and multiple interacting drivers.

Separate Random Forest models were developed for each agricultural zone and for each response variable (CR and RD). Predictor variables included five groups: event characteristics (drought/flood duration and intensity), phase-specific meteorology (precipitation, solar radiation, and air temperature separately for drought and flood phases), crop phenology (pre-/post-heading at event onset), large-scale climate background (mean SOI during the event and in the pre-event period), and static environmental/management factors (soil texture, porosity, elevation, slope, and irrigation status) (Table 2).

For each model, the dataset was split into training and testing subsets, and hyperparameters were optimized using cross-validation. Model performance was evaluated on the held-out test set using the coefficient of determination (R^2). SHAP values were then computed to quantify both the relative importance and directional influence of each predictor on CR and RD within each agricultural zone, thereby providing an interpretable attribution of zone-specific drivers. Additional details on model configuration, hyperparameter tuning, and performance evaluation are provided in Supplementary Text S4.

3. Results

3.1. Event identification: spatiotemporal patterns and trends of DTF events in maize regions

DTF hazards are highly uneven across China's maize belt, with most pixels experiencing only rare transitions but a small set of hotspots carrying a disproportionate share of exposure (Fig. 4a). At the pixel scale, occurrence is dominated by low frequencies: most grid cells experienced no more than three DTF events during 2000–2019, while high-frequency pixels occupy only a small fraction of the maize belt (Fig. 4a). Importantly, the three hazard dimensions—frequency, intensity, and duration—do not co-locate, meaning that "where DTF happens often" is not necessarily "where DTF is strongest " or "where it lasts longest " (Fig. 4a1–a3). Frequency per unit area is highest in Zone B (1.2) and relatively high in Zone I (0.9 events); Zones A/D/G are ~0.7 events, while Zones C/F are ~0.6 events (Fig. 4a1). Mean intensity ranges from 3.8 to 5.4, peaking in Zone I (5.4) and remaining high in Zone A (5.3), with the lowest intensity in Zone F (3.8) (Fig. 4a2). Mean duration spans 51–67 days, with the longest duration in Zone A (67 days), followed by Zone I (63 days) and Zone D (62 days), while Zone F is the shortest (51 days) (Fig. 4a3). This spatial "decoupling across hazard metrics" underscores why a single indicator (e.g., frequency alone) would miss key regional contrasts in within-season drought–flood

Table 2
Description of predictor variables used to explain the CR and RD of crops.

Category	Driver	Period	Abbreviation	Unit
Crop	Mean GPP	Multiple growth stages	GPP_{mean}	g C m^{-2} $8d^{-1}$
Soil	Silt content	Long-term static	Silt	%
	Clay content	Long-term static	Clay	%
	Soil porosity	Long-term static	Porosity	% by volume
Topography	Elevation	Long-term static	Elevation	m
	Slope	Long-term static	Slope	°
Large-scale Climate	Mean SOI (event)	Event period	SOI_{event}	
	Mean SOI (pre-event)	3 months pre-event	$SOI_{pre\text{-}event}$	
Local Meteorology	Total precipitation	Drought phase	$PREC_{drought}$	mm
		Flood phase	$PREC_{flood}$	mm
	Mean solar radiation	Drought phase	$SRAD_{drought}$	W m^{-2}
		Flood phase	$SRAD_{flood}$	W m^{-2}
	Mean air temperature	Drought phase	$TEMP_{drought}$	K
		Flood phase	$TEMP_{flood}$	K
Management	Irrigation status	Per growing season	Rainfed Irrigated	Binary (0/1)
Crop Phenology	Phenological stage	At event onset	Pre-heading/ Post-heading	Binary (0/1)
Event Characteristics	Drought intensity	Drought phase	$Intensity_{drought}$	
	Drought duration	Drought phase	$Duration_{drought}$	days
	Flood intensity	Flood phase	$Intensity_{flood}$	
	Flood duration	Flood phase	$Duration_{flood}$	days

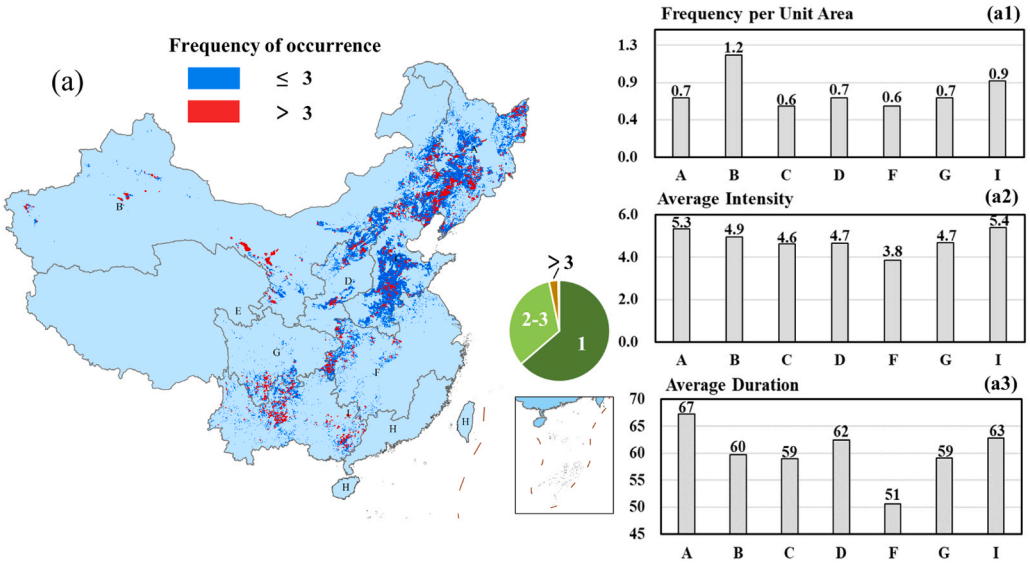

Fig. 4. Soil-moisture-defined DTF events in China's maize regions (2000–2019). (a) Spatial distribution of total event frequency. (a1–a3) Zone-level frequency per unit area, mean intensity, and mean duration. Note: Statistics are pooled over 2000–2019 (not annualized). Zone frequency sums pixel-level event counts; intensity and duration are averaged across all pixel–event records.

risks.

Temporal trends show that intensification is geographically concentrated rather than nationwide (Table 3). Zone G exhibits a significant increase in event frequency (Sen's slope = 14.55 events, $p < 0.05$), accompanied by significant increases in intensity (0.185, $p < 0.001$) and duration (1.70 days, $p < 0.01$). Zone I likewise shows significant positive trends in frequency (21.25 events, $p < 0.01$), intensity (0.301, $p < 0.01$), and duration (2.55 days, $p < 0.01$). Other zones show mixed slope estimates that are not statistically significant.

Table 3
Sen's slope estimates of regional trends in maize DTF event frequency, intensity, and duration. Note: Statistical significance: $p < 0.05$ (*); $p < 0.01$ (**); $p < 0.001$ (***).

	Sen's slope		
Zone	Frequency	Intensity	Duration
China	68.64	0.003	0.21
A	8.75	-0.024	-0.07
B	34.96	0.052	0.53
C	-28.36	-0.111	-0.66
D	4.68	0.024	0.15
F	-4.18	-0.014	-0.15
G	14.55*	0.185***	1.70**
I	21.25**	0.301**	2.55**

In summary, DTF exposure is generally low at the pixel level, but hazard "hotspots" and intensifying zones exist; notably, concurrent increases in frequency, intensity, and duration are largely confined to Zones G and I, indicating localized but substantial hazard amplification.

3.2. Crop response under sequential stress: spatial patterns and trends of impactful events, CR, and RD

DTF exposure does not automatically translate into photosynthetic damage: only a subset of events produces clear drought-stage GPP decline and becomes "crop-impactful". Fig. 5a therefore focuses on

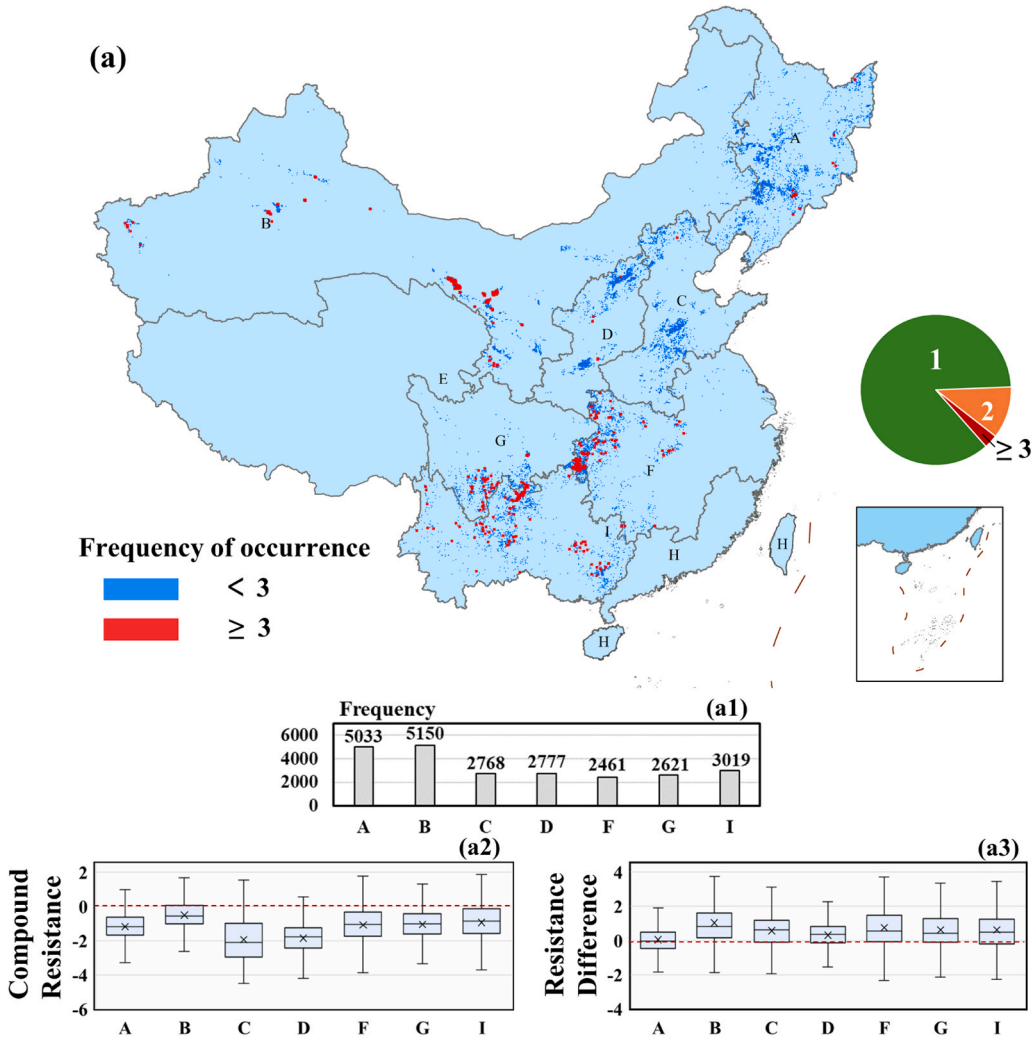

Fig. 5. Crop-impactful DTF events and maize photosynthetic responses in China's maize regions (2000–2019). (a) Spatial distribution of crop-impactful events. (a1–a3) Zone-level event frequency, CR, and RD. Note: Statistics are pooled over 2000–2019 (not annualized). Frequency sums pixel-level event counts; CR and RD are summarized as boxplots across all pixel–event records.

"crop-impactful events" (DTF events accompanied by a marked drought-stage GPP decline; criteria in Methods) and quantifies outcomes using CR and RD, moving from hazard exposure to realized crop consequences. Impactful-event counts are highly uneven, revealing where DTF becomes a realized crop stressor rather than a mere hydroclimatic transition (Fig. 5a1). Zones B and A record the largest counts (5150 and 5033 events), followed by Zone I (3019 events), Zone D (2777 events), Zone C (2768 events), Zone G (2621 events), and Zone F (2461 events). Across all zones, CR remains negative, indicating that sequential drought–flood stress consistently suppresses GPP overall; however, suppression is strongest in Zones C and D (more negative CR distributions), highlighting a clear geography of heightened vulnerability (Fig. 5a2). RD reveals the key "recovery vs compounding" split: most zones are dominated by positive RD (net flood-phase mitigation), whereas Zone A shows a mixed RD distribution with both positive and negative values—evidence that the flood phase can either relieve or deepen suppression depending on local conditions (Fig. 5a3).

Trend analysis further separates "more events" from "changing sensitivity", showing that event frequency and response metrics do not move in lockstep (Table 4). Nationally, crop-impactful event frequency increases significantly (Sen's slope = 62.13 events, $p < 0.01$), with significant increases in Zones A (10.36 events, $p < 0.01$), G (7.98 events, $p < 0.01$), and I (9.64 events, $p < 0.001$). Meanwhile, CR trends diverge regionally: it increases significantly (indicating an improvement in resistance) in Zones A/D/F/G/I (all $p < 0.001$) but decreases significantly (indicating a worsening of resistance) in Zones B/C (both $p < 0.001$). RD trends are also zone-opposing, decreasing significantly in Zones A and D (both $p < 0.001$) but increasing significantly in Zone B ($p < 0.05$) and Zones F/G/I (all $p < 0.001$).

Table 4
Sen's slope estimates of regional trends in maize crop-impactful event frequency, CR, and RD. Note: Statistical significance: $p < 0.05$ (*); $p < 0.01$ (**); $p < 0.001$ (***).

	Sen's slope		
Zone	Frequency	CR	RD
China	62.13**	-0.00011	-0.00641
A	10.36**	0.00010***	-0.00005***
B	3.78	-0.00011***	0.00003*
C	0.90	-0.00027***	-0.00003
D	0.27	0.00059***	-0.00026***
F	0.37	0.00011***	0.00033***
G	7.98**	0.00018***	0.00024***
I	9.64***	0.00028***	0.00022***

Juxtaposing Fig. 4 and Fig. 5 makes the central message explicit: hazard exposure and realized crop impact are decoupled, implying that regional context co-determines whether DTF becomes damaging (and whether the flood phase mitigates or compounds stress). Zone B exhibits

the highest exposure coupled with the largest number of impactful events. Zone A, despite only moderate exposure, still ranks among the highest in impactful event counts. Conversely, Zone I shows relatively high exposure but fewer impactful events than Zones A and B. This comparison demonstrates that regional context co-shapes the final crop-impact pattern, independent of event occurrence alone.

Overall, impactful events concentrate in Zones A and B, yet the geography of realized impact is distinct: the strongest whole-sequence suppression (most negative CR) clusters in Zones C and D, while RD is predominantly positive across most zones but becomes highly heterogeneous (spanning both signs) in Zone A, signaling that post-drought flooding can either mitigate or compound drought legacy depending on local conditions. These contrasts motivate a synthesis of DTF exposure, whole-sequence suppression (CR), and flood-phase net effect (RD) into three vulnerability archetypes—compounding-trap (Zone B), conditional-response (Zone A), and buffered-recovery (Zone I)—which we interpret mechanistically and translate into region-tailored adaptation priorities in Section 4.

3.3. What shapes the geography of CR?

To move from "where suppression is strong" to "what controls it", we modeled CR using Random Forest and interpreted drivers with SHAP, achieving robust explanatory skill (test-set $R^2 = 0.56–0.87$ across zones).

3.3.1. Relative importance of driving factors

Across zones, a consistent pattern emerges: phase-specific meteorology—especially flood-phase energy and thermal conditions—dominates the explanation of CR variability (Fig. 6). Zone A is led by flood-phase solar radiation and flood-phase air temperature, followed by drought-phase temperature and event-scale SOI. Zone B is dominated by flood-phase solar radiation, with drought-phase solar radiation and drought-phase precipitation ranked highly. Zone C similarly emphasizes solar radiation in both phases and includes flood-phase precipitation, drought-phase temperature, and pre-event SOI among key drivers. Zone D features flood-phase precipitation and flood-phase temperature, together with high importance of pre-event and event-scale SOI and elevation. Zones F and I emphasize flood duration and flood-phase solar radiation alongside phenological stage, while Zone G highlights flood-phase solar radiation and drought duration, accompanied by flood duration/precipitation and phenology. In contrast, management (rainfed vs irrigated) and many static background variables (soil texture fractions, slope) are consistently low-ranked, suggesting that CR geography is captured more by event-phase conditions than by static context within this framework (Fig. 6).

3.3.2. Dependency relationships of key drivers

SHAP dependency curves reveal predominantly nonlinear controls with thresholds and plateaus, indicating that CR is often "gated" rather than linearly driven by climate and event traits (Fig. 7). Here, positive SHAP values indicate association with higher CR (weaker suppression),

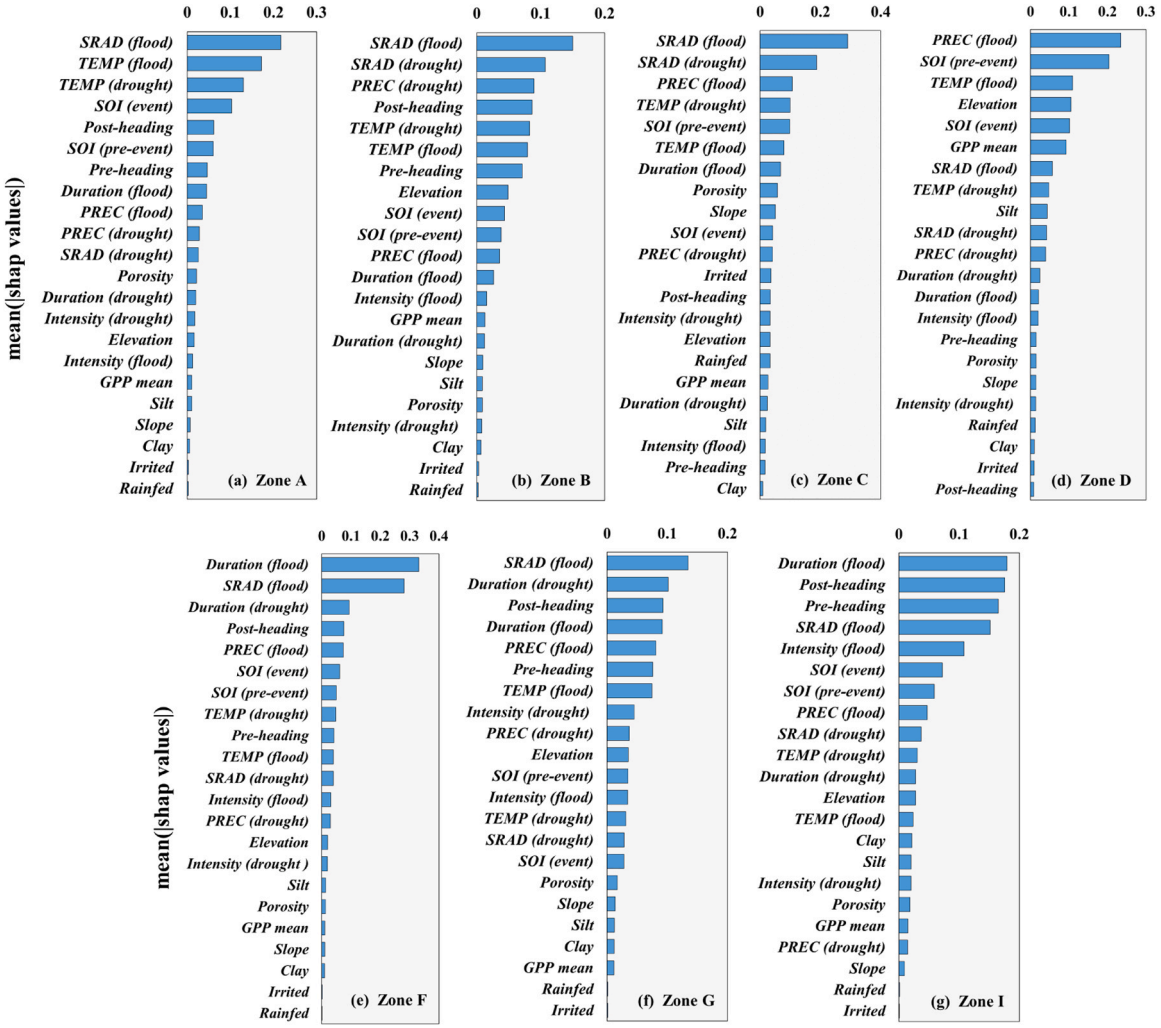

Fig. 6. SHAP-based relative importance of predictors for maize CR across agricultural zones. Predictors are ranked by mean absolute SHAP values.

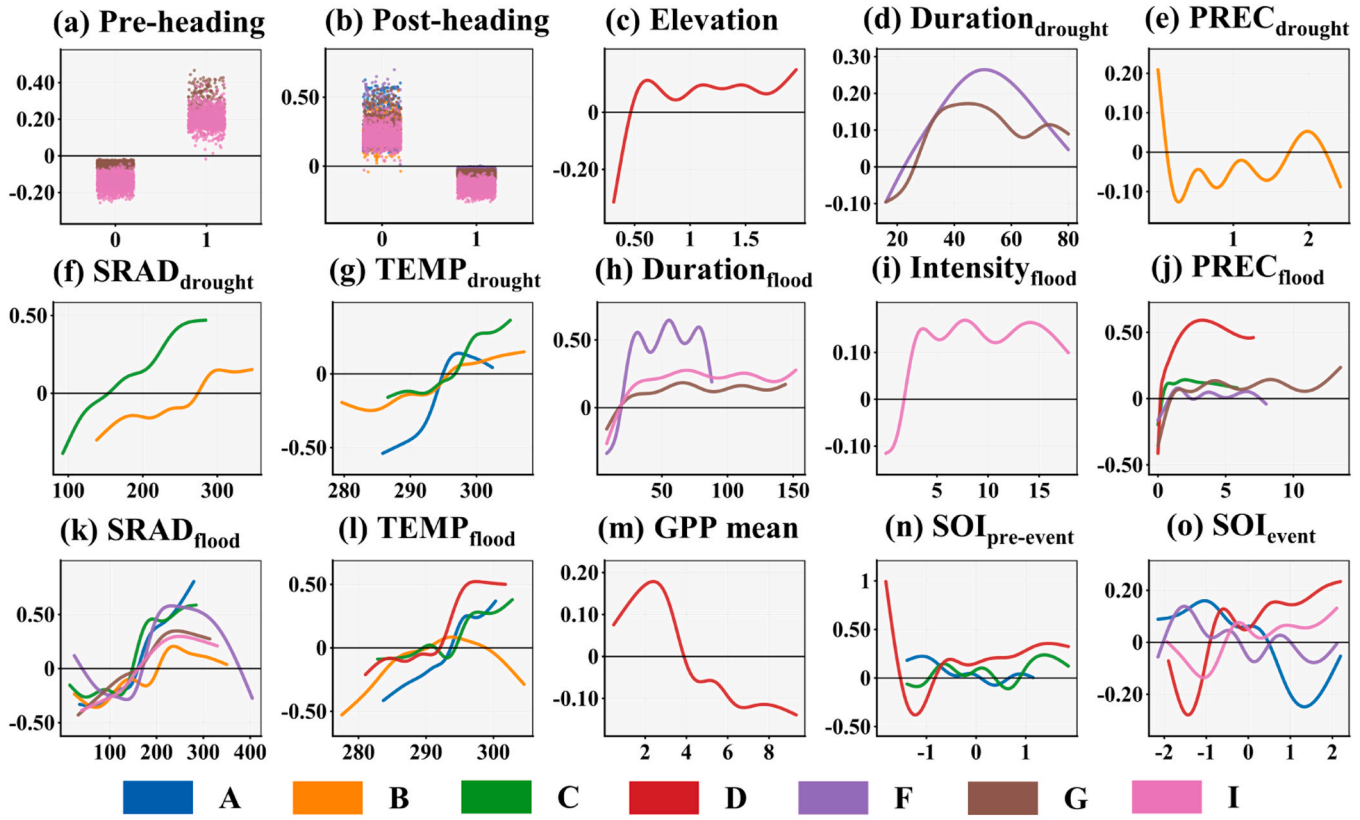

Fig. 7. SHAP dependence of zone-specific top drivers of maize CR across agricultural zones. X-axis: driver value; Y-axis: SHAP value; curves are fitted relationships. Note: For each zone, the top six drivers (by SHAP importance) were selected; a curve is shown only for zones where the driver is in the top six (colors denote zones), so single-curve panels indicate zone-specific drivers.

whereas negative values indicate lower CR (stronger suppression). Relationships are predominantly nonlinear and frequently show threshold or plateau behavior.

Phenological stage exhibits a clear categorical contrast: pre-heading corresponds to positive contributions, while post-heading corresponds to negative contributions. For continuous drivers, drought duration shows heterogeneous shapes, including hump-shaped responses (e.g., Zones F and G) and declining contributions in other regions. Drought precipitation (Zone B) is strongly positive only at extremely low values and then rapidly shifts into a negative regime with oscillations. Drought solar radiation rises with radiation in Zones B/C and levels off at higher values, while drought temperature shows pronounced regional contrasts (e.g., shifting from negative to positive in Zone A but declining toward negative at the warm end in Zone C).

Flood-stage drivers show comparable threshold behavior. Flood duration in Zones F/G/I shifts from negative/near-zero contributions at short durations to sustained positive contributions at longer durations (with stronger mid-range variability in Zone F). Flood intensity in Zone I transitions rapidly from negative to positive and plateaus. Flood precipitation differs sharply among zones (e.g., persistently positive in Zone D but predominantly negative and undulating in Zone A). Flood solar radiation typically shifts from negative at low values to positive at intermediate–high values, with zone-specific high-end behavior; flood temperature is nonlinear and zone-dependent. Mean GPP in Zone D decreases from positive to negative contributions with increasing values. Both SOI metrics show oscillatory, non-monotonic patterns with strong zone-to-zone differences.

Overall, CR geography reflects coupled drought-stage constraints and flood-stage modulation, strongly gated by phenology and, in some zones, influenced by SOI background—manifesting as threshold-, plateau-, and oscillation-type nonlinearities rather than a single universal driver.

3.4. *What explains the geography of the RD?*

RD is designed to isolate the net flood-phase contribution, so it is expected to be more phase-sensitive than CR—and the models confirm this with adequate skill for attribution (test-set R^2 = 0.43–0.83 across zones).

3.4.1. *Relative importance of driving factors*

Unlike CR, RD shows sharper zone-to-zone contrasts and clearer "phase preference", revealing where drought-stage constraints dominate versus where flood-stage energy/thermal conditions determine recovery (Fig. 8). Zone A is dominated by drought duration; Zone B by drought precipitation; Zone C by drought solar radiation together with both SOI metrics; Zone D by event-scale and pre-event SOI, along with drought temperature and mean GPP. In the southwest, flood-stage controls become prominent: Zones F and I rank flood solar radiation and flood duration among leading drivers, and Zone I additionally elevates phenological stage. Zone G remains led by drought solar radiation while flood solar radiation is also highly ranked. As with CR, management and many static soil/topographic variables remain low-ranked relative to event-process and large-scale background drivers.

3.4.2. *Dependency relationships of key drivers*

RD dependency curves exhibit frequent sign switches and saturation, directly visualizing how the flood phase can flip from "mitigating" to "compounding" depending on phase-specific conditions (Fig. 9). Drought duration declines with increasing duration in Zones A/B/C/D/G, rapidly shifting from near-zero/positive contributions to a stable negative plateau at longer durations. Drought intensity in Zone F drops quickly from positive to negative contributions. Drought precipitation (Zone B) is strongly positive only at extremely low values and then rapidly shifts to negative with oscillations. Drought temperature shows

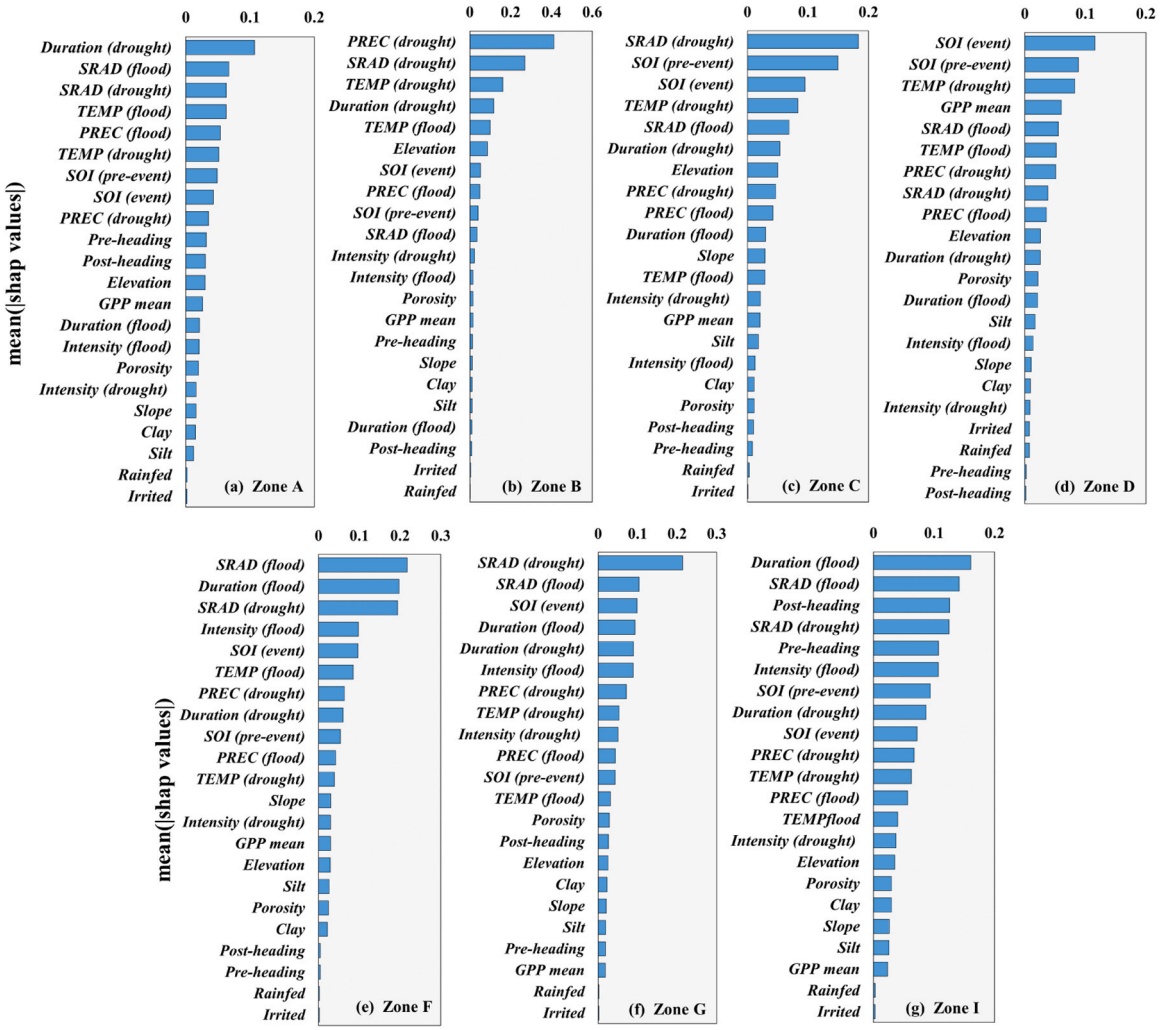

Fig. 8. SHAP-based relative importance of predictors for maize RD across agricultural zones. Predictors are ranked by mean absolute SHAP values.

strong regional contrasts: contributions rise at the warm end in Zone B but decline toward negative in Zone C; Zone A remains close to zero and fluctuates. Elevation in Zone B is non-monotonic, and phenological stage in Zone I shows a clear directional contrast (pre-heading positive vs post-heading negative).

Flood duration in Zones F/G/I shifts from negative/near-zero to sustained positive contributions, while flood intensity in Zones D/F/I transitions from negative to positive and plateaus. Flood precipitation in Zone A remains predominantly negative and undulating. Flood solar radiation typically shifts from negative at low values to positive at intermediate–high values with zone-specific high-end behavior; flood temperature is nonlinear. Mean GPP in Zone D decreases from positive to negative contributions with increasing values. Both SOI metrics retain oscillatory, non-monotonic relationships with strong zone-to-zone differences.

Overall, RD provides direct evidence for why the net flood-phase effect diverges across regions: different zones are dominated by drought-stage constraints, flood-stage processes, or SOI background, and sign transitions/plateaus indicate strong thresholds in whether rewetting aids recovery or compounds stress—consistent with RD's diagnostic intent.

4. Discussion

4.1. Climatic gradients shape a spatial continuum of vulnerability and archetypal response pathways

The spatial continuum of maize vulnerability to DTF across China's maize belt is largely shaped by pronounced climatic gradients and by the alignment of DTF timing with regional hydrothermal windows (i.e., concurrent radiation–temperature conditions and water availability during the flood phase) (Xie et al., 2025). Along the climatic gradient from the arid north to the temperate northeast and the subtropical southwest (Ren et al., 2023), systematic differences in hydrothermal regimes and seasonality dictate the flood-phase outcome: it can either subsidize water to offset drought or introduce secondary constraints like energy limitation (from cool/cloudy weather) or waterlogging stress (Durand et al., 2021). This macroclimatic backdrop offers a coherent explanatory framework for the divergent crop responses observed, explaining why geographically comparable DTF exposures translate into distinct vulnerability archetypes and response pathways—a finding consistent with the phase-specific meteorological controls revealed by our attribution analysis.

Our results reveal a spatial continuum of maize vulnerability to DTF across China's maize belt, underpinned by climatic gradients in aridity and in the energy–water balance that DTF events encounter during the flood phase. We highlight Zones C and D as impact hotspots (most negative CR) and leverage Zones B and I as contrasting mechanistic

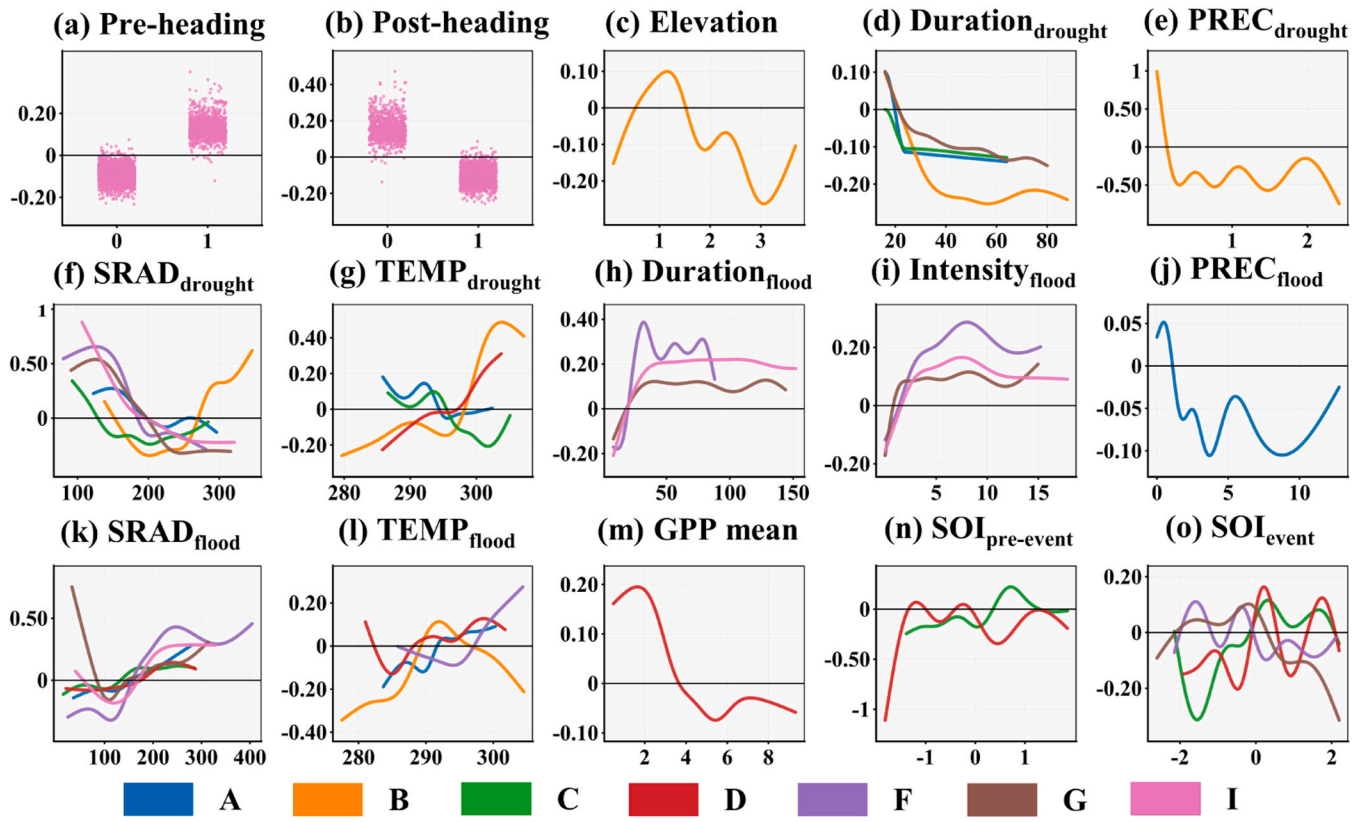

Fig. 9. SHAP dependence of zone-specific top drivers of maize RD across agricultural zones. X-axis: driver value; Y-axis: SHAP value; curves are fitted relationships. Note: For each zone, the top six drivers (by SHAP importance) were selected; a curve is shown only for zones where the driver is in the top six (colors denote zones), so single-curve panels indicate zone-specific drivers.

anchors to interpret the continuum. This continuum essentially contrasts regions where the background climate and flood-phase hydrothermal window typically allow flooding to alleviate drought limitation and support rebound, against those where flooding more frequently introduces secondary constraints such as waterlogging or energy limitation.

In the arid–semiarid north (Zone B), the prevailing climate—characterized by high atmospheric aridity and low soil water-holding capacity—predisposes crops to acute drought stress, thereby amplifying drought legacy and rendering recovery highly contingent on flood-phase hydrothermal condition (Kukal et al., 2023; Naorem et al., 2023; Su et al., 2025). This climatic predisposition helps explain why high DTF exposure (Fig. 4a1) coincides with a compounding stress trap: strong integrated suppression and a deteriorating resistance trend (Table 4). Within this setting, rapid wetting often fails to translate into recovery, as drought-adapted, drainage-limited systems can convert heavy rainfall into transient waterlogging and oxygen stress (Datta and Jong, 2002; Houk et al., 2006; Singh, 2018). The dominance of flood-phase meteorology in our attribution (Fig. 6) corroborates this, indicating that resilience strategies optimized for drought may become maladaptive when the system abruptly shifts to excess water. At the opposite end of the continuum, the warmer and more humid subtropical plateau climate of the southwest (Zone I) supports a buffered recovery pathway. Here, favorable baseline thermal and moisture conditions reduce the likelihood that flood phases coincide with strongly energy-limited or chilling windows, with complex topography providing additional modulation. Consequently, flood-phase moisture more readily supports physiological rebound (Zhang et al., 2019; Zhu et al., 2020), consistent with the observed higher resistance (less negative CR; Fig. 5a2) and the positive contributions of flood-phase temperature and longer flood duration (Fig. 6). In this climate, longer wet periods thus function as a sustained recharge window rather than a stress trigger.

Between these endpoints, other zones (notably C and D) occupy high-risk segments where integrated suppression is strongest (Fig. 5a2). Their vulnerability reflects a distinct climatic conjunction: a strong drought legacy coincides with flood-phase hydrothermal constraints—often cool/cloudy conditions and/or excess-water stress—that stall recovery. This aligns with the dominance of phase-specific meteorology over static background factors in explaining resistance patterns (Fig. 6), underscoring the primacy of climate-mediated, event-scale conditions in shaping ultimate impact. This interpretation also helps explain why flood-phase solar radiation and temperature emerged as dominant predictors in the SHAP analysis. Rewetting alone does not guarantee recovery; rather, the post-drought period must coincide with an energetically and thermally permissive window that allows renewed carbon uptake. In this sense, flood-phase solar radiation and temperature are not simply correlated weather variables, but proximate controls on whether recovery is physiologically possible. This is consistent with broader evidence that dry–wet transition dynamics under climate warming are shaped not only by water redistribution, but also by associated changes in energy availability and atmospheric demand (Chen and Wang, 2022).

4.2. *Conditional flood-phase effects and management levers for resilience*

RD isolates the flood phase's net contribution, and its spatial structure reveals when rewetting acts as recovery versus when it fails to translate into carbon-uptake gains. In most zones, RD is predominantly positive (Fig. 5a3), indicating that rewetting often provides net compensatory effects consistent with pulse-driven recovery dynamics (Chen et al., 2009; Feldman et al., 2021; Goodwell et al., 2018; Huxman et al., 2004). This does not imply weak vulnerability; rather, it suggests that flood-phase relief can be present yet still insufficient to offset the preceding drought legacy that governs the integrated response.

A key exception is the bimodal RD distribution in Zone A (Fig. 5a3), which indicates a conditional response regime: the flood phase alternates between helping and compounding depending on concurrent meteorological conditions. In Zone A, SHAP identifies flood-phase solar radiation and temperature as dominant controls of RD (Fig. 8), and dependency patterns show that low radiation/temperature corresponds to neutral or negative contributions (Fig. 9). This supports a process-based explanation: when floods coincide with cool, cloudy conditions typical of late-season periods, photosynthetic recovery becomes energy- and thermally constrained and the rewetting benefit is muted or reversed (Bhattacharya, 2022; Li et al., 2024; Mu et al., 2010). The bimodality therefore reflects not just flood occurrence, but the historical co-occurrence of floods with both favorable and unfavorable radiation–temperature states in this region. These RD-based process diagnostics naturally translate into distinct leverage points for adaptation: mitigating excess-water stress in compounding-trap regions, avoiding energy-limited flood windows in conditional-response regions, and preserving buffering capacity where recovery is already resilient.

Accordingly, adaptation priorities should be tailored to the dominant response pathway. For compounding-trap settings (e.g., Zone B), the priority is to prevent rapid wetting from becoming a secondary stressor. This argues for upgrading drought-centric irrigation toward systems that also reduce waterlogging risk—for example, integrating efficient irrigation (sprinkler/drip) with subsurface drainage or drainage-friendly field engineering to decouple water inputs from oxygen stress (Chanson, 2024; Lazović et al., 2024). In such regions, forecast-informed operations can further reduce exposure by adjusting water storage and field conditions ahead of likely transitions (Shi et al., 2026). For conditional-response regions (e.g., Zone A), the actionable lever is not "more water", but flood-phase energy/thermal constraints. Strategies include microclimate and phenological adaptation: soil warming practices (e.g., film mulching) and cultivar/sowing-date adjustments that reduce the likelihood that flood phases coincide with low radiation/temperature windows during sensitive late-season periods (Ding et al., 2016; Mari et al., 2024; Nouri et al., 2017; Zhao et al., 2015; Zhou et al., 2020).

For buffered-recovery regions (e.g., Zone I), the priority is to preserve and amplify existing buffering rather than overhaul systems. Ecosystem-based measures that stabilize microclimate/hydrology (e.g., maintaining landscape buffers) combined with precision management (monitoring-driven irrigation/fertilization) can maximize compensatory growth during favorable windows with minimal disruption (Aishwarya et al., 2025; Anderson-Teixeira et al., 2012; Li et al., 2022; Lloret et al., 2021; Swift et al., 2004). These management implications should, however, be interpreted as biophysically informed directions rather than as a full socio-economic or operational adaptation assessment. The present framework identifies where hydroclimatic conditions tend to favor compensation versus compounding, but it does not fully resolve how infrastructure, institutional capacity, and farmer decision-making mediate realized losses and adaptation success.

4.3. Uncertainty, robustness, and methodological scope

Several sources of uncertainty should be considered when interpreting the present framework. First, DTF identification is definition-dependent, and recent work has shown that threshold choice and temporal aggregation can materially alter the detection, timing, and inferred impacts of consecutive drought–flood events (Anderson et al., 2025). In this study, however, event definition was designed to serve crop-impact diagnosis rather than a purely hydrological event inventory. Because canopy GPP was available as an 8-day composite and represents an averaged physiological state over that interval, we used 8-day aggregated soil moisture to define persistent drought and flood states, thereby matching the temporal support of the hazard indicator to that of the crop-response metric. At the same time, to reduce the risk of missing rapid transitions, we introduced daily soil moisture through the SMCI-based abruptness confirmation step. This dual-timescale framework does not remove definitional uncertainty altogether, but it represents an effort to balance state robustness and rapid-transition detection under the spatiotemporal constraints of regional crop-impact analysis. More broadly, regional crop-impact analysis is constrained by a practical trade-off: variables that reasonably capture crop-state dynamics across large areas often do not simultaneously provide field-scale temporal precision. Our approach therefore prioritizes consistency between hazard diagnosis and crop-response observation, while using the daily-scale abruptness test to partially recover transition information that would otherwise be smoothed in 8-day composites.

Second, the low importance of irrigation in the SHAP analysis should not be interpreted as evidence that management is unimportant (Götte and Brunner, 2024). In the present model, irrigation was represented only as a static binary variable, which can capture broad management background but cannot resolve dynamic regulation, drainage operations, reservoir buffering, or event-specific interventions. More broadly, the archetypes identified here should be interpreted as biophysical response archetypes rather than complete risk archetypes. In regions such as Zone B, the compounding stress trap therefore likely reflects not only unfavorable hydroclimatic windows, but also socio-economic and infrastructural constraints that are not explicitly resolved in the current framework (Matanó et al., 2022).

Third, uncertainty remains in the flood-phase GPP signal. The PML-based GPP product used here is a model-derived dataset rather than a direct pixel-level physiological observation (Zhang et al., 2019), and uncertainty may increase during flood phases characterized by persistent cloud cover and heavy precipitation. In addition, part of this uncertainty may already propagate from interpolation or model-based reconstruction in the input variables used to generate the final product. Because an independent pixel-level QA band was not available for direct event screening, we addressed this issue through a robustness analysis rather than strict QA masking. Specifically, we recalculated an alternative CR-type metric by retaining the drought-phase GPP percentile trajectory, excluding the internal flood-phase GPP values, and replacing the original flood-end value with the GPP percentile from the subsequent 8-day period. This test was restricted to events for which the post-flood 8-day interval still fell within the maize growing season, so events extending beyond the seasonal boundary were not included in the comparison. The original and alternative metrics remained positively correlated in all zones, with generally high sign consistency in most regions, indicating that the main regional contrasts do not depend exclusively on a single flood-end composite (Fig. S1; Table S1). However, agreement was weaker in Zone D than in the other zones, implying stronger endpoint sensitivity there. This robustness analysis cannot eliminate uncertainty in the flood-phase GPP signal, but it helps show that the principal interpretation is not solely an artifact of the original flood-end definition.

Finally, the $>40\%$ pre-drought GPP threshold used to define crop-impactful events is a pragmatic screening rule rather than a uniquely correct universal cutoff (Zhang et al., 2025). Alternative thresholds are plausible across different agro-ecological settings, so we evaluated the sensitivity of event screening to alternative baseline thresholds. Across alternative pre-drought GPP thresholds (30%–50%), event counts decreased systematically with increasing threshold stringency, as expected, but the main regional contrasts remained stable (Fig. S2; Table S2). In particular, the regional pattern of mean CR was unchanged across all tested thresholds, while the broad spatial structure of mean RD was also preserved. No major reversal in the principal regional interpretation was observed across agricultural zones. These results indicate that the main regional conclusions are not an artifact of the selected 40% baseline threshold, even though sample size is sensitive to threshold choice.

4.4. Limitations and future perspectives

Several limitations qualify interpretation. First, 1-km data enable nationwide inference but can smooth field-scale heterogeneity in drainage, soil, and management, potentially underestimating localized extremes such as waterlogging hotspots. Second, defining "crop-impactful" events via acute GPP decline captures short-term photosynthetic depression but may miss longer-lived injuries or allocation shifts that influence yield. Third, attribution identifies statistical associations rather than causal mechanisms, so inferred processes (e.g., chilling/low-radiation gating of recovery, waterlogging constraints) require experimental validation. Future work can extend this framework in three directions: (i) ground-truthing inferred mechanisms through multi-scale observations and experiments (e.g., UAV/IoT monitoring coupled with manipulations), (ii) integrating flood-phase recovery and compound-stress damage functions into process-based crop models (e.g., APSIM/DSSAT) where recovery is often weakly represented, and (iii) testing generality across crops and compound extremes (e.g., heat–drought) to evaluate whether the proposed archetypes represent transferable principles of crop resilience.

5. Conclusion

This study provides a process-explicit, national-scale diagnosis of maize photosynthetic vulnerability to drought-to-flood (DTF) transitions across China during 2000–2019. DTF hazards were highly heterogeneous, with frequency, intensity, and duration showing clear spatial decoupling and significant intensification concentrated in the Sichuan Basin and the Yunnan–Guizhou Plateau. However, exposure did not directly predict impact: the strongest whole-event suppression, captured by compound resistance (CR), occurred in the North China Plain and the Loess Plateau rather than in the highest-frequency regions. The flood phase was typically mitigative but strongly conditional. Resistance difference (RD) showed that rewetting generally alleviated drought legacy, whereas in the Northeast China Plain its effect weakened and could even become negative under low flood-phase radiation and temperature, indicating energy-limited recovery.

More broadly, maize responses to DTF were governed mainly by nonlinear, phase-specific meteorological constraints, whereas irrigation played a secondary role in the current framework. Integrating exposure, CR, and RD further revealed three vulnerability archetypes—compounding-trap, conditional-response, and buffered-recovery—distinguished by differences in flood-phase effectiveness. Overall, the CR–RD framework separates whole-event suppression from the net contribution of the flood phase and provides a scalable basis for diagnosing regional biophysical vulnerability and informing region-tailored adaptation across China's maize belt. Sensitivity and robustness analyses further showed that the principal regional contrasts were broadly stable under alternative pre-drought GPP thresholds and an alternative flood-end representation, although uncertainty in flood-phase GPP and the omission of broader socio-economic and infrastructural factors mean that the framework should be interpreted as a diagnosis of biophysical vulnerability rather than a complete risk assessment.

CRediT authorship contribution statement

Qiang Yu: Writing – review & editing, Funding acquisition. **Jianqiang He:** Writing – review & editing, Conceptualization. **Sen Chen:** Writing – review & editing. **Peng Li:** Writing – original draft, Visualization, Software, Methodology. **Ning Yao:** Writing – review & editing. **Liang He:** Writing – review & editing, Funding acquisition, Conceptualization. **Meichen Feng:** Writing – review & editing. **Chao Wang:** Writing – review & editing. **Xingyu Hao:** Writing – review & editing.

Declaration of Competing Interest

The authors declare that they have no known competing financial interests or personal relationships that could have appeared to influence the work reported in this paper.

Acknowledgements

This work was supported by the National Natural Science Foundation of China (No. 42375195).

Appendix A. Supporting information

Supplementary data associated with this article can be found in the online version at doi:10.1016/j.agwat.2026.110381.

Data availability

Data will be made available on request.

References

Aishwarya, Kumar, A., Kumar, P., 2025. Sensors-Based Irrigation for Increasing Crop and Water Productivity. In: Kumar, A., Singh, V.K., Singh, Y., Singh, S.K., Kumar, P. (Eds.), Modern Technology for Sustainable Agriculture. Springer Nature Switzerland, Cham, pp. 101–113. https://doi.org/10.1007/978-3-031-88396-5_8.

Anderson, B.J., Muñoz-Castro, E., Tallaksen, L.M., Matano, A., Götte, J., Armitage, R., Magee, E., Brunner, M.I., 2025. What is a drought-to-flood transition? Pitfalls and recommendations for defining consecutive hydrological extreme events. Hydrol. Earth Syst. Sci. 29, 6069–6092. https://doi.org/10.5194/hess-29-6069-2025.

Anderson-Teixeira, K.J., Snyder, P.K., Twine, T.E., Cuadra, S.V., Costa, M.H., DeLucia, E. H., 2012. Climate-regulation services of natural and agricultural ecoregions of the Americas. Nat. Clim. Change 2, 177–181. https://doi.org/10.1038/nclimate1346.

Bai, X., Zhao, C., Tang, Y., Zhang, Z., Yang, B., Wang, Z., 2023. Identification, physical mechanisms and impacts of drought–flood abrupt alternation: a review. Front. Earth Sci. 11. https://doi.org/10.3389/feart.2023.1203603.

Bai, X., Wang, Z., Wu, J., Zhang, Z., Zhang, P., 2024. A novel multivariate multiscale index for drought-flood abrupt alternations: Considering precipitation, evapotranspiration, and soil moisture. J. Hydrol. 643, 132039. https://doi.org/10.1016/j.jhydrol.2024.132039.

Bhattacharya, A., 2022. Effect of Low Temperature Stress on Photosynthesis and Allied Traits: A Review. In: Bhattacharya, A. (Ed.), Physiological Processes in Plants Under Low Temperature Stress. Springer, Singapore, pp. 199–297. https://doi.org/10.1007/978-981-16-9037-2_3.

Bi, W., Li, M., Weng, B., Yan, D., Dong, Z., Feng, J., Wang, H., 2023a. Drought-flood abrupt alteration events over China. Sci. Total Environ. 875, 162529. https://doi.org/10.1016/j.scitotenv.2023.162529.

Bi, W., Weng, B., Yan, D., Zhang, D., Liu, C., Shi, X., Jing, L., Yan, S., Wang, H., 2023b. Response of summer maize growth to drought-flood abrupt alternation. Front. Earth Sci. 11. https://doi.org/10.3389/feart.2023.1086769.

Bi, W., Hu, Y., Weng, B., Zhang, D., Wang, F., Lin, W., Wang, W., Dong, G., Yan, D., 2025. Drought–flood abrupt alternation events increase soil nitrogen loss via surface runoff in a typical grain base in China. J. Hydrol. Reg. Stud. 60, 102543. https://doi.org/10.1016/j.ejrh.2025.102543.

Chan, S.K., Bindlish, R., O'Neill, P., Jackson, T., Njoku, E., Dunbar, S., Chaubell, J., Piepmeier, J., Yueh, S., Entekhabi, D., Colliander, A., Chen, F., Cosh, M.H., Caldwell, T., Walker, J., Berg, A., McNairn, H., Thibeault, M., Martínez-Fernández, J., Uldall, F., Seyfried, M., Bosch, D., Starks, P., Holifield Collins, C., Prueger, J., van der Velde, R., Asanuma, J., Palecki, M., Small, E.E., Zreda, M., Calvet, J., Crow, W.T., Kerr, Y., 2018. Development and assessment of the SMAP enhanced passive soil moisture product. Remote Sens. Environ. 204, 931–941. https://doi.org/10.1016/j.rse.2017.08.025.

Chanson, H., 2024. Low-head hydraulic structures in irrigation and drainage engineering: challenging operation and design implications. J. Irrig. Drain. Eng. 150, 03124001. https://doi.org/10.1061/JIDEDH.IRENG-10288.

Chen, H., Wang, S., 2022. Accelerated transition between dry and wet periods in a warming climate. Geophys. Res. Lett. 49, e2022GL099766. https://doi.org/10.1029/2022GL099766.

Chen, S., Lin, G., Huang, J., Jenerette, G.D., 2009. Dependence of carbon sequestration on the differential responses of ecosystem photosynthesis and respiration to rain pulses in a semiarid steppe. Glob. Change Biol. 15, 2450–2461. https://doi.org/10.1111/j.1365-2486.2009.01879.x.

Datta, K.K., Jong, C., de, 2002. Adverse effect of waterlogging and soil salinity on crop and land productivity in northwest region of Haryana, India. Agric. Water Manag 57, 223–238. https://doi.org/10.1016/S0378-3774(02)00058-6.

Ding, D.Y., Feng, H., Zhao, Y., He, J.Q., Zou, Y.F., Jin, J.M., 2016. Modifying winter wheat sowing date as an adaptation to climate change on the Loess Plateau. Agron. J. 108, 53–63. https://doi.org/10.2134/agronj15.0262.

Durand, M., Murchie, E.H., Lindfors, A.V., Urban, O., Aphalo, P.J., Robson, T.M., 2021. Diffuse solar radiation and canopy photosynthesis in a changing environment. Agric. For. Meteor. 311, 108684. https://doi.org/10.1016/j.agrformet.2021.108684.
Feldman, A.F., Short Gianotti, D.J., Konings, A.G., Gentine, P., Entekhabi, D., 2021. Patterns of plant rehydration and growth following pulses of soil moisture availability. Biogeosciences 18, 831–847. https://doi.org/10.5194/bg-18-831-2021.
Forzieri, G., Dakos, V., McDowell, N.G., Ramdane, A., Cescatti, A., 2022. Emerging signals of declining forest resilience under climate change. Nature 608, 534–539. https://doi.org/10.1038/s41586-022-04959-9.
Gao, Y., Hu, T., Yuan, H., Yang, J., 2017. Analysis on yield reduced law of rice in Huaibei plain under drought-flood abrupt alternation. Trans. Chin. Soc. Agric. Eng. 33 (21), 128–136.
Gao, Y., Hu, T., Wang, Q., Yuan, H., Yang, J., 2019. Effect of drought–flood abrupt alternation on rice yield and yield components. Crop Sci. 59, 280–292. https://doi.org/10.2135/cropsci2018.05.0319.
Ge, C., Sun, P., Yao, R., Zhang, Y., Shen, H., Yang, H., 2025. Drivers of ecological drought recovery: Insights from meteorological and soil drought impact. J. Hydrol. 646, 132324. https://doi.org/10.1016/j.jhydrol.2024.132324.
Goodwell, A.E., Kumar, P., Fellows, A.W., Flerchinger, G.N., 2018. Dynamic process connectivity explains ecohydrologic responses to rainfall pulses and drought. Proc. Natl. Acad. Sci. 115, E8604–E8613. https://doi.org/10.1073/pnas.1800236115.
Götte, J., Brunner, M.I., 2024. Hydrological Drought-To-Flood Transitions Across Different Hydroclimates in the United States. Water Resour. Res. 60, e2023WR036504. https://doi.org/10.1029/2023WR036504.
Gu, B., Zhou, S., Yu, B., Findell, K.L., Lintner, B.R., 2025. Multifaceted changes in water availability with a warmer climate. Npj Clim. Atmos. Sci. 8, 31. https://doi.org/10.1038/s41612-025-00913-4.
Hamed, K.H., Ramachandra Rao, A., 1998. A modified Mann-Kendall trend test for autocorrelated data. J. Hydrol. 204, 182–196. https://doi.org/10.1016/s0022-1694(97)00125-x.
Han, J., Fang, S., Wang, X., Zhuo, W., Yu, Y., Peng, X., Zhang, Y., 2024. The impact of intra-annual temperature fluctuations on agricultural temperature extreme events and attribution analysis in mainland China. Sci. Total Environ. 949, 174904. https://doi.org/10.1016/j.scitotenv.2024.174904.
Hao, Z., Hao, F., Xia, Y., Feng, S., Sun, C., Zhang, X., Fu, Y., Hao, Y., Zhang, Y., Meng, Y., 2022. Compound droughts and hot extremes: Characteristics, drivers, changes, and impacts. Earth-Sci. Rev. 235, 104241. https://doi.org/10.1016/j.earscirev.2022.104241.
He, J., Yang, K., Tang, W., Lu, H., Qin, J., Chen, Y., Li, X., 2020. The first high-resolution meteorological forcing dataset for land process studies over China. Sci. Data 7, 25. https://doi.org/10.1038/s41597-020-0369-y.
Houk, E., Frasier, M., Schuck, E., 2006. The agricultural impacts of irrigation induced waterlogging and soil salinity in the Arkansas Basin. Agric. Water Manag 85, 175–183. https://doi.org/10.1016/j.agwat.2006.04.007.
Huang, J., Hu, T., Yasir, M., Gao, Y., Chen, C., Zhu, R., Wang, X., Yuan, H., Yang, J., 2019. Root growth dynamics and yield responses of rice (Oryza sativa L.) under drought—Flood abrupt alternating conditions. Environ. Exp. Bot. 157, 11–25. https://doi.org/10.1016/j.envexpbot.2018.09.018.
Huang, S., Gan, Y., Wang, C., Wang, S., Chen, J., Zhang, X., Chen, Z., Gu, X., Xia, J., Chen, N., Gong, J., 2026. Urbanization-induced compression effect accelerates and amplifies dry-wet abrupt alternations in Chinese cities. Sci. Bull. https://doi.org/10.1016/j.scib.2026.01.078.
Huxman, T.E., Snyder, K.A., Tissue, D., Leffler, A.J., Ogle, K., Pockman, W.T., Sandquist, D.R., Potts, D.L., Schwinning, S., 2004. Precipitation pulses and carbon fluxes in semiarid and arid ecosystems. Oecologia 141, 254–268. https://doi.org/10.1007/s00442-004-1682-4.
Jacques, C., Salon, C., Barnard, R.L., Vernoud, V., Prudent, M., Jacques, C., Salon, C., Barnard, R.L., Vernoud, V., Prudent, M., 2021. Drought stress memory at the plant cycle level: a review. Plants 10. https://doi.org/10.3390/plants10091873.
Konkathi, P., Karthikeyan, L., 2024. Utility of L-band and X-band vegetation optical depth to examine vegetation response to soil moisture droughts in South Asia. Remote Sens. Environ. 301, 113933. https://doi.org/10.1016/j.rse.2023.113933.
Kukal, M.S., Irmak, S., Dobos, R., Gupta, S., 2023. Atmospheric dryness impacts on crop yields are buffered in soils with higher available water capacity. Geoderma 429, 116270. https://doi.org/10.1016/j.geoderma.2022.116270.
Lazović, N., Mulaomerović-Šeta, A., Kalajdžisalihović, H., Džubur, A., 2024. Reconstruction and Improvement of Surface Drainage Systems as a Preventive Flood Protection Measure. In: Ademović, N., Akšamija, Z., Karabegović, A. (Eds.), Advanced Technologies, Systems, and Applications IX. Springer Nature Switzerland, Cham, pp. 3–18. https://doi.org/10.1007/978-3-031-71694-2_1.
Li, J., Bai, X., Ran, F., Zhang, C., Yan, Y., Li, P., Chen, H., 2024. Effects of combined extreme cold and drought stress on growth, photosynthesis, and physiological characteristics of cool-season grasses. Sci. Rep. 14, 116. https://doi.org/10.1038/s41598-023-49531-1.
Li, P., He, L., Wang, X., Ding, E., Yu, Q., 2025. How reliable are long time-series reanalysis and model-based soil moisture products for agricultural soil water stress monitoring? Insights from a five-dataset evaluation across China. Agric. Water Manag 320, 109845. https://doi.org/10.1016/j.agwat.2025.109845.
Li, Q., Shi, G., Shangguan, W., Nourani, V., Li, J., Li, L., Huang, F., Zhang, Y., Wang, C., Wang, D., Qiu, J., Lu, X., Dai, Y., 2022. A 1 km daily soil moisture dataset over China using in situ measurement and machine learning. Earth Syst. Sci. Data 14, 5267–5286. https://doi.org/10.5194/essd-14-5267-2022.
Liang, L., Xia, J., Wang, Z., 2025. Dynamics of dry-to-wet abrupt alternation events in mainland China from 1961 to 2022: A novel identification method integrating daily soil moisture and precipitation. J. Hydrol. Reg. Stud. 60, 102520. https://doi.org/10.1016/j.ejrh.2025.102520.
Lloret, J., Sendra, S., García-Fernández, J., García, L., Jimenez, J.M., Lloret, J., Sendra, S., García-Fernández, J., García, L., Jimenez, J.M., 2021. A WiFi-Based Sensor Network for Flood Irrigation Control in Agriculture. Electronics 10. https://doi.org/10.3390/electronics10202454.
Luo, Y., Zhang, Z., Chen, Y., Li, Z., Tao, F., 2020. ChinaCropPhen1km: a high-resolution crop phenological dataset for three staple crops in China during 2000–2015 based on leaf area index (LAI) products. Earth Syst. Sci. Data 12, 197–214. https://doi.org/10.5194/essd-12-197-2020.
Mari, J.A., Soothar, R.K., Thidar, M., Mangrio, M.A., Mirjat, M.U., Katohar, I., 2024. Effect of plastic film mulch and irrigation water regimes on soil temperature pattern, plant growth and water productivity of maize. Ecol. Front 44, 752–759. https://doi.org/10.1016/j.ecofro.2024.02.007.
Matanó, A., de Ruiter, M.C., Koehler, J., Ward, P.J., Van Loon, A.F., 2022. Caught between extremes: understanding human-water interactions during drought-to-flood events in the Horn of Africa. Earths Future 10, e2022EF002747. https://doi.org/10.1029/2022EF002747.
Mu, H., Jiang, D., Wollenweber, B., Dai, T., Jing, Q., Cao, W., 2010. Long-term Low Radiation Decreases Leaf Photosynthesis, Photochemical Efficiency and Grain Yield in Winter Wheat. J. Agron. Crop Sci. 196, 38–47. https://doi.org/10.1111/j.1439-037X.2009.00394.x.
Naorem, A., Jayaraman, S., Dang, Y.P., Dalal, R.C., Sinha, N.K., Rao, C.S., Patra, A.K., Naorem, A., Jayaraman, S., Dang, Y.P., Dalal, R.C., Sinha, N.K., Rao, C.S., Patra, A. K., 2023. Soil Constraints in an Arid Environment—Challenges, Prospects, and Implications. Agronomy 13. https://doi.org/10.3390/agronomy13010220.
Ning, Y., Nunes, J.P., Zhou, J., Baartman, J., dos Santos, F.M., Liu, X., Ma, L., Ritsema, C. J., Chen, X., 2026. Forty-year data analysis of droughts and drought-flood dynamics: impacts of cascading reservoirs. J. Hydrol. 668, 134957. https://doi.org/10.1016/j.jhydrol.2026.134957.
Nouri, M., Homaee, M., Bannayan, M., Hoogenboom, G., 2017. Towards shifting planting date as an adaptation practice for rainfed wheat response to climate change. Agric. Water Manag 186, 108–119. https://doi.org/10.1016/j.agwat.2017.03.004.
Peduzzi, P., Dao, H., Herold, C., Mouton, F., 2009. Assessing global exposure and vulnerability towards natural hazards: the Disaster Risk Index. Nat. Hazards Earth Syst. Sci. 9, 1149–1159. https://doi.org/10.5194/nhess-9-1149-2009.
Piao, S., Zhang, X., Chen, A., Liu, Q., Lian, X., Wang, X., Peng, S., Wu, X., 2019. The impacts of climate extremes on the terrestrial carbon cycle: A review. Sci. China Earth Sci. 62, 1551–1563. https://doi.org/10.1007/s11430-018-9363-5.
Pissolato, M.D., Martins, T.S., Fajardo, Y.C.G., Souza, G.M., Machado, E.C., Ribeiro, R.V., 2024. Stress memory in crops: what we have learned so far. Theor. Exp. Plant Physiol. 36, 535–565. https://doi.org/10.1007/s40626-024-00315-6.
Qiu, J., He, C., Liu, X., Gao, L., Tan, C., Wang, X., Kong, D., Wigneron, J.-P., Chen, D., Xia, J., 2024. Projecting dry-wet abrupt alternation across China from the perspective of soil moisture. Npj Clim. Atmos. Sci. 7, 269. https://doi.org/10.1038/s41612-024-00808-w.
Ren, H., Wen, Z., Liu, Y., Lin, Z., Han, P., Shi, H., Wang, Z., Su, T., 2023. Vegetation response to changes in climate across different climate zones in China. Ecol. Indic. 155, 110932. https://doi.org/10.1016/j.ecolind.2023.110932.
Shi, G., Sun, W., Shangguan, W., Wei, Z., Yuan, H., Li, L., Sun, X., Zhang, Y., Liang, H., Li, D., Huang, F., Li, Q., Dai, Y., 2025. A China dataset of soil properties for land surface modelling (version 2, CSDLv2). Earth Syst. Sci. Data 17, 517–543. https://doi.org/10.5194/essd-17-517-2025.
Shi, H., Cai, X., Hu, X., Jamal, A., Li, D., Sun, C., Liang, X.-Z., 2026. A sub-seasonal to seasonal climate forecast informed irrigation scheduling tool for the Contiguous United States. Environ. Model. Softw. 197, 106819. https://doi.org/10.1016/j.envsoft.2025.106819.
Shi, W., Huang, S., Liu, D., Huang, Q., Han, Z., Leng, G., Wang, H., Liang, H., Li, P., Wei, X., 2021. Drought-flood abrupt alternation dynamics and their potential driving forces in a changing environment. J. Hydrol. 597, 126179. https://doi.org/10.1016/j.jhydrol.2021.126179.
Singh, A., 2018. Alternative management options for irrigation-induced salinization and waterlogging under different climatic conditions. Ecol. Indic. 90, 184–192. https://doi.org/10.1016/j.ecolind.2018.03.014.
Su, Z., Yu, Z., Gu, Z., Zhao, D., Peng, J., 2025. Unravelling the hidden drivers of crop sensitivity to precipitation in the arid and semi-arid regions of Northwest China. Agric. Water Manag 320, 109866. https://doi.org/10.1016/j.agwat.2025.109866.
Sun, W., Zhou, S., Yu, B., Zhang, Y., Keenan, T., Fu, B., 2025. Soil moisture-atmosphere interactions drive terrestrial carbon-water trade-offs. Commun. Earth Environ. 6, 169. https://doi.org/10.1038/s43247-025-02145-z.
Swift, M.J., Izac, A.-M.N., van Noordwijk, M., 2004. Biodiversity and ecosystem services in agricultural landscapes—are we asking the right questions? Agric. Ecosyst. Environ. Environ. Serv. Land Use Chang. Bridg. Gap Policy Res. Southeast Asia 104, 113–134. https://doi.org/10.1016/j.agee.2004.01.013.
Toca, A., Gonzalez-Benecke, C.A., Nelson, A.S., Jacobs, D.F., 2025. Drought memory expression varies across ecologically contrasting forest tree species. Environ. Exp. Bot. 231, 106094. https://doi.org/10.1016/j.envexpbot.2025.106094.
Tu, X., Pang, W., Chen, X., Lin, K., Liu, Z., 2022. Limitations and improvement of the traditional assessment index for drought-wetness abrupt alternation. Adv. Water Resour. Adv. Water Resour. 33 (4), 592–601. https://doi.org/10.14042/j.cnki.32.1309.2022.04.007.
Wang, L., Yuan, Z., Shi, X., Yin, J., Qin, T., Zhang, J., 2025. A driving force analysis method for drought-flood abrupt alternation events. Ecol. Inf. 90, 103214. https://doi.org/10.1016/j.ecoinf.2025.103214.
Ward, P.J., Blauhut, V., Bloemendaal, N., Daniell, J.E., de Ruiter, M.C., Duncan, M.J., Emberson, R., Jenkins, S.F., Kirschbaum, D., Kunz, M., Mohr, S., Muis, S., Riddell, G. A., Schäfer, A., Stanley, T., Veldkamp, T.I.E., Winsemius, H.C., 2020. Review article:

natural hazard risk assessments at the global scale. Nat. Hazards Earth Syst. Sci. 20, 1069–1096. https://doi.org/10.5194/nhess-20-1069-2020.

Xie, L., Li, Y., Zhang, Z., Siddique, K.H.M., Song, X., 2025. Exploring the combined effects of drought and drought-flood abrupt alternation on vegetation using interpretable machine learning model and r-vine copula function. Agric. For. Meteor. 370, 110568. https://doi.org/10.1016/j.agrformet.2025.110568.

Xiong, Q., Deng, Y., Zhong, L., 2018. Effects of drought-flood abrupt alternation on yield and physiological characteristics of rice. Int. J. Agric. Biol. 20 (5), 44, 1107-1116 ref.

Xu, H., Yuan, H., Zhang, H., Jiang, S., Liu, J., 2021. The effect of drought-floods abrupt alternation on the growth and development of soybean in branching stage. Water Sav. Irrig. Jieshui Guangai No. 12, 70–74, 80.

Yuan, H., Peng, Z., Yang, J., Liu, J., Zhao, H., Ning, S., Xu, X., A, R., Li, H., Yuan, H., Peng, Z., Yang, J., Liu, J., Zhao, H., Ning, S., Xu, X., A, R., Li, H., 2024. Effects of Alternative Stress of Drought–Flood on Summer Maize Growth and Yield. Water 16. https://doi.org/10.3390/w16192742.

Zhang, D., Tong, S., Qi, Q., Zhang, M., An, Y., Wang, X., Lu, X., 2019. Effects of drought and re-flooding on growth and photosynthesis of *Carex schmidtii* Meinsh: Implication for tussock restoration. Ecol. Indic. 103, 134–144. https://doi.org/10.1016/j.ecolind.2019.04.005.

Zhang, G., Wang, H., Gan, T.Y., Zhang, S., Zhao, J., Su, X., Fu, X., Shi, L., Xu, P., Lu, M., Wang, C., 2025. A comprehensive review of recent progress on the drought-flood abrupt alternation. J. Hydrol. 661, 133806. https://doi.org/10.1016/j.jhydrol.2025.133806.

Zhang, K., Zhao, Z., Tian, F., 2026. Mitigating the impact of increased drought-flood abrupt alternation events under climate change: the role of reservoirs in the Lancang-Mekong River Basin. Hydrol. Earth Syst. Sci. 30, 671–691. https://doi.org/10.5194/hess-30-671-2026.

Zhang, L., Xie, Y., Zhu, X., Ma, Q., Brocca, L., 2024. CIrrMap250: annual maps of China's irrigated cropland from 2000 to 2020 developed through multisource data integration. Earth Syst. Sci. Data 16, 5207–5226. https://doi.org/10.5194/essd-16-5207-2024.

Zhang, M., Yuan, X., Zeng, Z., Pan, M., Wu, P., Xiao, J., Keenan, T.F., 2025. A pronounced decline in northern vegetation resistance to flash droughts from 2001 to 2022. Nat. Commun. 16, 2984. https://doi.org/10.1038/s41467-025-58253-z.

Zhang, Y., Kong, D., Gan, R., Chiew, F.H.S., McVicar, T.R., Zhang, Q., Yang, Y., 2019. Coupled estimation of 500 m and 8-day resolution global evapotranspiration and gross primary production in 2002–2017. Remote Sens. Environ. 222, 165–182. https://doi.org/10.1016/j.rse.2018.12.031.

Zhang, Y., You, Q., Ullah, S., Chen, C., Shen, L., Liu, Z., 2023. Substantial increase in abrupt shifts between drought and flood events in China based on observations and model simulations. Sci. Total Environ. 876, 162822. https://doi.org/10.1016/j.scitotenv.2023.162822.

Zhao, J., Yang, X., Dai, S., Lv, S., Wang, J., 2015. Increased utilization of lengthening growing season and warming temperatures by adjusting sowing dates and cultivar selection for spring maize in Northeast China. Eur. J. Agron. 67, 12–19. https://doi.org/10.1016/j.eja.2015.03.006.

Zheng, S., Weng, B., Bi, W., Yan, D., Ren, L., Wang, H., 2025. Significant increase and escalation of drought-flood abrupt alteration in China's future. Agric. Water Manag 312, 109449. https://doi.org/10.1016/j.agwat.2025.109449.

Zhou, L., Zhao, W., Yang, R., Feng, H., 2020. Soil temperature modeling in topsoil with plastic film mulching and low spring temperatures. Arch. Agron. Soil Sci. 66, 1936–1947. https://doi.org/10.1080/03650340.2019.1702163.

Zhu, R., Wu, F., Zhou, S., Hu, T., Huang, J., Gao, Y., 2020. Cumulative effects of drought–flood abrupt alternation on the photosynthetic characteristics of rice. Environ. Exp. Bot. 169, 103901. https://doi.org/10.1016/j.envexpbot.2019.103901.